

MODELING THE VISCOSITY OF SILICATE MELTS CONTAINING MANGANESE OXIDE

W.-Y. Kim, A. D. Pelton, C. W. Bale, E. Bélisle, S. A. Deeterov[#]

École Polytechnique, Dép. de Génie Chimique, Centre de Recherche en Calcul Thermochimique (CRCT),
Montréal, Québec, Canada

(Received 18 September 2013; accepted 15 July 2013)

Abstract

Our recently developed model for the viscosity of silicate melts is applied to describe and predict the viscosities of oxide melts containing manganese oxide. The model requires three pairs of adjustable parameters that describe the viscosities in three systems: pure MnO, MnO–SiO₂ and MnO–Al₂O₃–SiO₂. The viscosity of other ternary and multicomponent silicate melts containing MnO is then predicted by the model without any additional adjustable model parameters. Experimental viscosity data are reviewed for melts formed by MnO with SiO₂, Al₂O₃, CaO, MgO, PbO, Na₂O and K₂O. The deviation of the available experimental data from the viscosities predicted by the model is shown to be within experimental error limits.

Keywords: Viscosity; Thermodynamic modeling; Silicates; Slags; Glass melts

1. Introduction

Viscosity is one of the key properties of slags, which influences the performance of pyrometallurgical processes in many ways. Slag used in the production of ferromanganese alloys has a large composition range depending on the manganese ore and its gangue minerals. It can contain up to 30 wt% MnO. By influencing the flow pattern in the furnace, the viscosity of slag in the ferromanganese alloy process has a great impact on the temperature distribution and reduction behavior of manganese oxide. The viscosity of slag must also be controlled to provide stable mass transfer at the slag/metal interface and heat transfer through the slag.

Recently we developed a new model for the viscosity of oxide melts [1-5]. In this model the viscosity is related to the structure of the melt, which in turn is calculated from the thermodynamic description of the melt using the Modified Quasichemical Model [6, 7]. Most importantly, the model takes into account the formation of the silica network which has a profound effect on the viscosity. The model predicts, within experimental error limits, the viscosity of multicomponent slags from just a few model parameters fitted to the viscosities of the binary and some ternary subsystems.

In the present study, viscosity data are reviewed for melts formed by MnO with SiO₂, Al₂O₃, CaO, MgO, Na₂O and K₂O. A few model parameters are

optimized to reproduce the viscosities of MnO, MnO–SiO₂ and MnO–Al₂O₃–SiO₂ melts. Then the available experimental viscosity data for other ternary and higher-order MnO-containing systems are compared to the viscosities calculated by the model without using any additional adjustable model parameters.

2. Viscosity model

For a more detailed description of the model, see the earlier articles [1-3]. A brief summary of the model similar to the one below was given earlier in References [8, 9].

2.1 Melts formed by SiO₂ and basic oxides MO_x

The structure of silicate melts is characterized by the bridging behavior of oxygen. An oxygen atom separating an M–M pair is a free oxygen, O²⁻; an oxygen separating an M–Si pair is a non-bridging oxygen, O⁻; and an oxygen separating a Si–Si pair is called a bridging oxygen, O⁰. The silicon atoms in silicate melts are always tetrahedrally bonded to four oxygen ions. Basic silicate melts consist mainly of Me^{nt}, O²⁻ and SiO₄⁴⁻ ions. As the silica content increases above the orthosilicate composition, the SiO₄⁴⁻ tetrahedra start to polymerize, forming more and more bridging oxygens, and gradually a three-dimensional network is formed. The structural changes taking place upon formation of the SiO₂

* Corresponding author: sergei.deeterov@polymtl.ca

network can be characterized by the amounts of so-called Q^i -species [10] which are defined as Si atoms linked to i bridging oxygens and $(4 - i)$ non-bridging oxygens. In pure SiO_2 all four oxygens surrounding each Si are bridging oxygens and the fraction of Q^4 -species is 1. An isolated SiO_4^{4-} ion is a Q^0 -species.

Over the past 25 years our group has been developing a thermodynamic database for silicate melts [11] using the Modified Quasichemical Model [6, 7]. The database currently contains over 20 elements and successfully models and predicts the thermodynamic properties of multicomponent silicate liquids. The model parameters stored in the thermodynamic database have been obtained by critical evaluation and optimization of all available experimental thermodynamic and phase diagram data. The Modified Quasichemical Model and the thermodynamic database can be used to calculate the numbers of M–M, M–Si and Si–Si second-nearest-neighbor pairs, which correspond to the fractions of free oxygens, broken bridges and bridging oxygens, as functions of temperature and composition.

Let us define p as the probability that a particular pair emanating from a given Si atom is a Si–Si pair. As a first approximation, we can assume that bonds are randomly distributed and that the probability p does not depend on the types of other pairs emanating from this Si atom. Hence, p can be calculated by dividing the number of Si–Si pairs emanating from all Si atoms by the number of all Si–Si and Si–M pairs:

$$p = \frac{2n_{\text{Si-Si}}}{2n_{\text{Si-Si}} + \sum_{\text{M}} n_{\text{Si-M}}} \quad (1)$$

where n_{i-j} is the number of i - j pairs. Note that every Si–Si pair is counted twice as emanating from one and from the other Si atom in the pair.

Then the probability that a given Si atom is a Q^4 -species is p^4 because four Si–Si pairs emanate from each Si atom. Similarly we can calculate the probabilities that a given Si atom is a Q^i -species as well as the fractions of all five Q^i -species in a melt.

A statistical method can be used to calculate the interconnectivity between Q^4 -species. The probability that a given Si atom is part of a cluster of at least n interconnected Si–Si pairs is proportional to p^n . This is only an approximate relation. Clearly there are restrictions on the arrangements of bonds because of the local structure of the melts which is similar to the diamond lattice structure of cristobalite. The approximation becomes better for larger values of n . In any case, the function p^n is clearly a measure of the connectivity of the network. We postulate that a certain critical cluster size can be defined that mimics the formation of a percolating SiO_2 network. When this cluster size is surpassed the viscosity increases dramatically. Our analysis of the viscosity data indicates that a group of 40 interconnected Si–Si pairs

is a good estimate for the critical cluster size.

The following equations were proposed [1-3] for the viscosity of liquid melts. (For melts containing simultaneously basic oxides and Al_2O_3 see Section B below.)

$$\ln \eta = A + \frac{E}{RT} \quad (2)$$

$$E = \sum_{\text{M}} (X_{\text{M}} E_{\text{M}}) + \sum_{\text{M}} (X_{\text{M}} X_{\text{Si}} E_{\text{M-Si}}) + \left. \begin{aligned} & E_{\text{Si}}^* + E_{\text{Si}}^E p^{40} + (p^4 - p^{40}) \frac{\sum_{\text{M}} (X_{\text{M}} E_{\text{M-Si}}^R)}{\sum_{\text{M}} X_{\text{M}}} + \\ & + X_{\text{Si}} \left\{ \begin{aligned} & \frac{\sum_{\text{M=Alkali}} (X_{\text{M}} E_{\text{M-Si}}^{\text{Ring}})}{\sum_{\text{M}} X_{\text{M}}} \\ & + p^7 (1-p)^3 \frac{\sum_{\text{M=Alkali}} (X_{\text{M}} E_{\text{M-Si}}^R)}{\sum_{\text{M}} X_{\text{M}}} \end{aligned} \right\} \end{aligned} \right\} \quad (3)$$

$$A = \sum_{\text{M}} (X_{\text{M}} A_{\text{M}}) + \sum_{\text{M}} (X_{\text{M}} X_{\text{Si}} A_{\text{M-Si}}) + \left. \begin{aligned} & A_{\text{Si}}^* + A_{\text{Si}}^E p^{40} + (p^4 - p^{40}) \frac{\sum_{\text{M}} (X_{\text{M}} A_{\text{M-Si}}^R)}{\sum_{\text{M}} X_{\text{M}}} \end{aligned} \right\} \quad (4)$$

where η is the viscosity in Pa·s, R is the gas constant, T is temperature in kelvins and X_{M} and X_{Si} are the cation mole fractions. For example, for a binary system $\text{Na}_2\text{O-SiO}_2$, the cation mole fractions of Na and Si are

$$X_{\text{Na}} = \frac{n_{\text{NaO}_{0.5}}}{n_{\text{NaO}_{0.5}} + n_{\text{SiO}_2}}; \quad X_{\text{Si}} = \frac{n_{\text{SiO}_2}}{n_{\text{NaO}_{0.5}} + n_{\text{SiO}_2}} \quad (5)$$

where n_i are the mole fractions of the components.

The model parameters A_{M} and E_{M} give the viscosity of the pure liquid oxides MO_x which are not network formers:

$$\ln \eta_{\text{MO}_x} = A_{\text{M}} + \frac{E_{\text{M}}}{RT} \quad (6)$$

Similarly, $\ln \eta_{\text{Si}}^* = A_{\text{Si}}^* + \frac{E_{\text{Si}}^*}{RT}$ represents the hypothetical viscosity of SiO_2 if it were like a basic oxide and did not form a network. An excess contribution per Si atom of large clusters of Q^4 -species, which contain at least 40 interconnected Si–Si pairs, is proportional to p^{40} . This contribution is represented by the parameters E_{Si}^E and A_{Si}^E . This is the contribution of the silica network which is assumed to be independent of other cations M. Therefore, the viscosity of pure SiO_2 is:

$$\ln \eta_{\text{Si}} = (A_{\text{Si}}^* + A_{\text{Si}}^E) + \frac{(E_{\text{Si}}^* + E_{\text{Si}}^E)}{RT} \quad (7)$$

An excess contribution per Si atom of the rest of the Q^4 -species, that is of smaller clusters which

contain less than 40 interconnected Si–Si pairs, is proportional to $(p^4 - p^{40})$. This contribution is represented by binary parameters E_{M-Si}^R and A_{M-Si}^R . Since these clusters are smaller, the M cations are located closer to a given Si atom so that the contribution of this Si atom depends on M.

The second terms in Eqs. (3) and (4) contain the additional binary parameters E_{M-Si} and A_{M-Si} to account for small nonlinearities of the viscosity, if any, as a function of composition in the basic regions of the binary systems M–Si.

It should be noted that parameters A_{M-Si}^R and A_{M-Si} are rarely required and can generally be set equal to zero. So far the model has been applied to multicomponent oxide liquids containing Si, B, Al, Ca, Mg, Li, Na, K, Mn, Ni, Fe^{2+} , Fe^{3+} , Pb, Zn, Ti. Only one non-zero parameter, A_{Al-Si}^R , was introduced and even in this case it improved the description only slightly.

Finally, E_{M-Si}^{Ring} is a binary parameter which is non-zero only for alkali oxide – silica systems. It accounts for an additional excess contribution of Q^2 - and Q^3 -species polymerized into large rings which have been reported to form in these systems based on evidence from NMR and Raman spectroscopy [12, 13]. It should be noted that a similar additional term was never needed in Eq. (4) for A . That is, all parameters $A_{M-Si}^{Ring} = 0$.

In summary, for most binary systems MO_x – SiO_2 only two binary parameters, E_{M-Si}^R and E_{M-Si} , were required to fit the experimental viscosity data, while for each alkali oxide – SiO_2 system one additional binary parameter, E_{M-Si}^{Ring} , was needed.

2.2 Taking into account the charge compensation effect

Certain amphoteric oxides such as Al_2O_3 can behave in profoundly different ways in a silicate melt depending on the overall composition. When added to a pure silica melt, Al_2O_3 acts as a network-modifier, breaking the oxygen bridges of the pure silica network, thereby substantially decreasing the viscosity. On the other hand, when equimolar amounts of MO or M_2O and Al_2O_3 are added to SiO_2 , some of the Al cations assume tetrahedral coordination and replace Si in the liquid network, so that Al acts as a network-former. The missing charge is compensated by M cations that stay close to the Al ions. Due to this “Charge Compensation Effect”, [10] there is a maximum in the viscosity when the molar ratio of Al_2O_3 to MO or M_2O is unity.

The thermodynamic database of Modified Quasichemical Model parameters, upon which the viscosity model is based, does not explicitly consider the different structural roles of Al. Hence, in order to model the viscosity maximum, the amount of network-forming Al must be evaluated *a posteriori*.

This is done as follows.

Consider, for example, the Al_2O_3 – CaO – Na_2O – SiO_2 system. We can write two reactions to form tetrahedrally-coordinated Al that enters the silica network and is charge-compensated by either Na or Ca:



It is assumed that the NaAl and $CaAl_2$ “species” have the same effect on the viscosity as one or two Si atoms respectively. The model parameters are simply the Gibbs energies of reactions (8) and (9). These Gibbs energies are not dependent on temperature, but are found to vary linearly as a function of SiO_2 content, becoming more negative at higher SiO_2 concentrations. Hence, only two parameters are required to model the Charge Compensation Effect in each ternary system MO_x – Al_2O_3 – SiO_2 (including the limiting MO_x – Al_2O_3 binary systems).

The equilibrium constants for reactions (8) and (9) can be written as

$$K_{NaAl} = \exp\left(\frac{-\Delta G_{NaAl}}{RT}\right) = \frac{X'_{NaAl}}{X'_{Na} X'_{Al}} \quad (10)$$

$$K_{CaAl_2} = \exp\left(\frac{-\Delta G_{CaAl_2}}{RT}\right) = \frac{X'_{CaAl_2}}{X'_{Ca} (X'_{Al})^2} \quad (11)$$

At each given overall composition X'_{Na} , X'_{Ca} , X'_{Al} and X'_{Si} , Eqs. (10) and (11) can be solved, taking into account the mass balance constraints, to calculate X'_{Na} , X'_{Ca} , X'_{Al} , X'_{Si} , X'_{NaAl} , and X'_{CaAl_2} .

Here $(X'_{NaAl} + 2X'_{CaAl_2})$ gives the amount of network-forming Al, while X'_{Al} gives the amount of network-modifying Al.

Since we assume that NaAl and $CaAl_2$ species have exactly the same effect on the viscosity as one or two Si atoms respectively, the viscosity can be calculated by substituting the following adjusted mole fractions into Eqs. (2), (3) and (4):

$$\begin{aligned} X_{Si}^* &= (X'_{Si} + X'_{NaAl} + 2X'_{CaAl_2}) / N_{tot}^* \\ X_{Al}^* &= X'_{Al} / N_{tot}^* \\ X_{Ca}^* &= X'_{Ca} / N_{tot}^* \\ X_{Na}^* &= X'_{Na} / N_{tot}^* \\ N_{tot}^* &= X'_{Na} + X'_{Ca} + X'_{Al} + X'_{Si} + X'_{NaAl} + 2X'_{CaAl_2} \end{aligned} \quad (12)$$

Clearly, this proposed treatment of the Charge Compensation Effect is a simplification. Strictly speaking, the charge-compensated Al that enters the silica network does not form chemically distinct species such as NaAl and $CaAl_2$; the contribution of network-forming Al to the viscosity may be different from that of Si, and, finally, mole fractions are used in Eqs. (10) and (11) instead of

activities. However, the proposed treatment gives a qualitatively correct functional dependence of the viscosity on temperature and composition and the description is made quantitative by fitting the Gibbs energies of reactions (8) and (9) to experimental viscosity data in the ternary $\text{MO}_x\text{-Al}_2\text{O}_3\text{-SiO}_2$ systems.

3. Review of available viscosity data and calibration of the model

In the present study, viscosity data are reviewed for all MnO-containing subsystems of the $\text{MnO-SiO}_2\text{-Al}_2\text{O}_3\text{-CaO-MgO-PbO-Na}_2\text{O-K}_2\text{O}$ system. The data judged to be most reliable are shown in the figures below.

The proposed model is intended for oxide melts. The extension of the model to describe the viscosity of glasses will be reported elsewhere. Consequently, the viscosity data were collected mainly for melts above the liquidus or for slightly supercooled melts where crystallization did not occur. These measurements were mostly made with rotational or vibrational viscometers. Phase equilibrium calculations were carried out using the FactSage thermochemical software and databases [11] to check that the viscosity was indeed measured in a single-phase liquid region. If an abnormally high viscosity value was reported for a temperature below the liquidus, this was most likely the result of crystallization. Viscosities of glasses, measured for example by a fiber elongation or a beam-bending method, were not considered in the present study.

Parameters of the model for MnO-containing melts that were fitted to the experimental viscosity data are listed in Table 1. The model parameters for melts without MnO were reported previously [1-3, 8, 9].

3.1 The accuracy and reliability of viscosity measurements

The difficulties associated with measurements of the viscosity of molten oxides over wide temperature and composition ranges arise from the simultaneous presence of the following conditions [14]:

- a very wide viscosity range;
- the poor heat conducting properties of the liquid;
- the invariable presence of small bubbles in the liquid;
- the very high temperatures at which the experiments must be carried out.

A rotational viscometer is most suitable for measurements under these conditions. The numerous sources of systematic errors related to the use of this particular type of viscometer and to the viscosity measurements of oxide melts in general are outlined, for example, in References [14] and [15]. When

viscosity measurements were carried out by some of the best laboratories in a "round robin" project [15] using the same reference materials, the average spread of data obtained by different laboratories was about 20%. The average accuracy of the data is probably no better than 50% when uncertainties in sample preparation and purity are taken into account.

For calibration and testing of the present viscosity model, experimental viscosity data were collected for the $\text{Al}_2\text{O}_3\text{-B}_2\text{O}_3\text{-CaO-MgO-FeO-Fe}_2\text{O}_3\text{-MnO-NiO-PbO-ZnO-Na}_2\text{O-K}_2\text{O-TiO}_2\text{-Ti}_2\text{O}_3\text{-SiO}_2\text{-F}$ system and its subsystems. From the scatter of the data measured by different authors for same systems, it can be concluded that the average absolute accuracy of viscosity measurements is probably about ± 0.5 to 1.0 in the natural logarithmic scale [1-5, 8, 9]. Of course the accuracy can be as high as ± 0.2 in the natural logarithmic scale for the best laboratories when samples are carefully prepared and characterized before and after the experiments. On the other hand, the real accuracy can be much lower for viscosity measurements at very high temperatures, for very corrosive or volatile melts, or outside the optimal range for a rotational viscometer [16] ($\ln(\text{Pa}\cdot\text{s})$ from -4 to 9).

3.2 Viscosities of the binary MnO-SiO₂ system

Due to its extremely high melting temperature, there are no viscosity data for pure liquid MnO. The viscosity of MnO-SiO₂ melts has been measured using the rotating crucible method with Pt-Rh crucibles under Ar atmosphere [16-19], a vibrational viscometer with iron crucibles under He atmosphere [20], the logarithmic decrement method with either Mo crucibles under H₂ atmosphere [21], or iron crucibles under (H₂+N₂) gas atmosphere [22, 23]. As can be seen from Fig. 1, the reported experimental

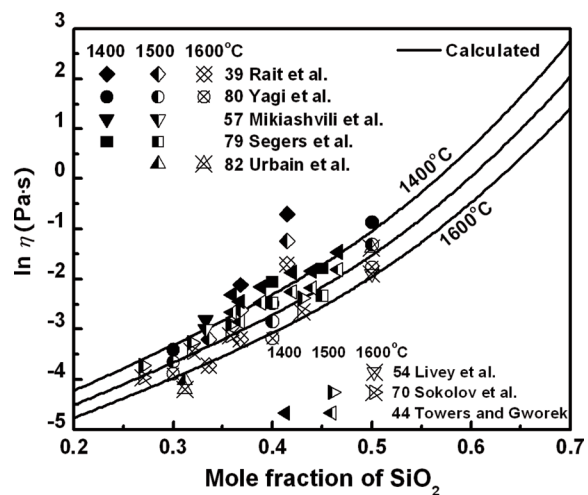


Figure 1. Viscosity of MnO-SiO₂ melts: experimental points [16-23] and calculated lines.

data are in good agreement except for the results of Rait et al. [21], which tend to be higher, although the difference is within experimental error limits. These data were used to obtain the parameters A_{Mn} and E_{Mn} describing the viscosity of pure liquid MnO as well as the binary MnO-SiO₂ parameters E_{Mn-Si} and E_{Mn-Si}^R . The optimized model parameters are given in Table 1. The agreement of the calculated lines with the experimental points shown in Fig. 1 is within the experimental scatter.

The model parameters for subsystems without MnO that are used for the viscosity calculations in the present study were optimized and reported elsewhere [1-3, 8].

3.3 Ternary melts without alumina

The viscosities of ternary melts without Al₂O₃ are predicted by the model based on the unary and binary viscosity parameters without any additional adjustable parameters. To test the predictive ability of the model, experimental viscosity data were compiled for all ternary melts formed by MnO with SiO₂, CaO, MgO, PbO, Na₂O and K₂O. To the best of our knowledge, experimental measurements have been reported only for MnO-CaO-SiO₂, MnO-Na₂O-SiO₂ and MnO-PbO-SiO₂ melts.

3.3.1 MnO-CaO-SiO₂

The viscosities of MnO-CaO-SiO₂ melts were measured by the rotating crucible method with Pt-Rh [17, 24], Pt [25], Mo [26] and iron [27] crucibles under Ar atmosphere at the compositions shown in Figure 2. Figures 3 to 9 compare the viscosities predicted by the model with the experimental data. The calculated viscosities are in excellent agreement with the most recent measurements by Sridhar et al. [27] (see Fig. 7) and with the results of Segers et al. [17], considering the scatter of the latter data which is obvious from Figs. 5 and 6. The viscosities reported by Kawahara et al. [25] are slightly lower than predicted by the model, but both the temperature and the composition dependence are in excellent agreement with the calculated lines. Mikiashvili et al. [24] observed a solid crystalline phase during their experiments which can explain the higher values of their viscosities.

At constant mole fraction of SiO₂, the model predicts an almost linear decrease of the viscosity

Table 1. Model parameters for the viscosity expressed in Pa.s.

System	Model parameter	Model parameters (J.mol ⁻¹)
MnO	$A_{Mn} = -9$	$E_{Mn} = 44040$
MnO-SiO ₂		$E_{Mn-Si} = -50000$ $E_{Mn-Si}^R = 81000$
MnO-Al ₂ O ₃ -SiO ₂		$\Delta G_{MnAl_2} = 14500 - 94500 X_{SiO_2}$ (where X_{SiO_2} is the mole fraction of SiO ₂)

when CaO is replaced by MnO as can be seen from Figs. 5 to 7. Overall, the viscosities of MnO-CaO-SiO₂ melts predicted by the model are in agreement with the experiments within experimental error limits.

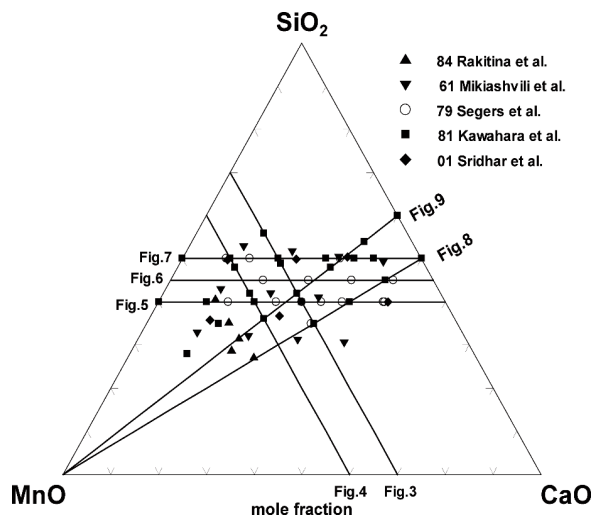


Figure 2. Compositions in the MnO-CaO-SiO₂ system at which experimental viscosity measurements are available [17, 24-27]. The lines indicate seven sections of this system selected to show the viscosity as a function of composition in Figs 3 to 9.

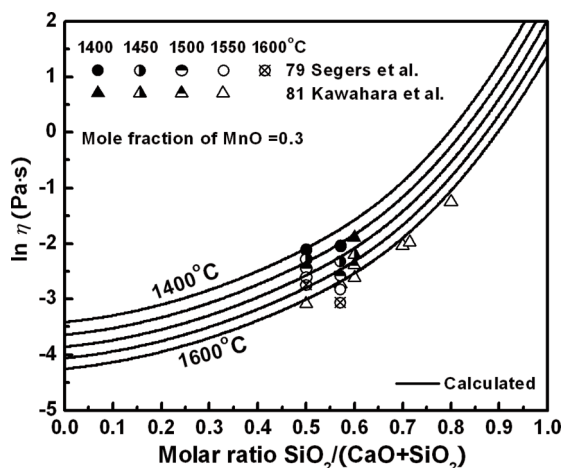


Figure 3. Viscosity of MnO-CaO-SiO₂ melts at 30 mol% MnO: experimental points [17, 25] and calculated lines.

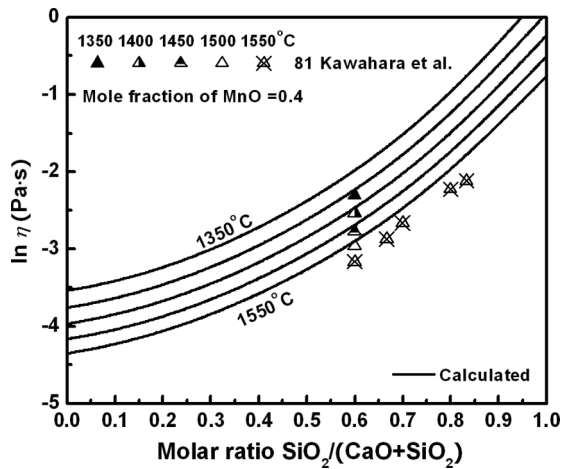


Figure 4. Viscosity of MnO-CaO-SiO₂ melts at 40 mol% MnO: experimental points [25] and calculated lines.

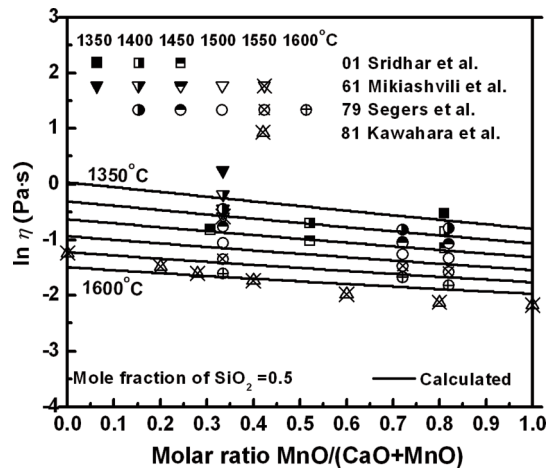


Figure 7. Viscosity of MnO-CaO-SiO₂ melts at 50 mol% SiO₂: experimental points [17, 24, 25, 27] and calculated lines.

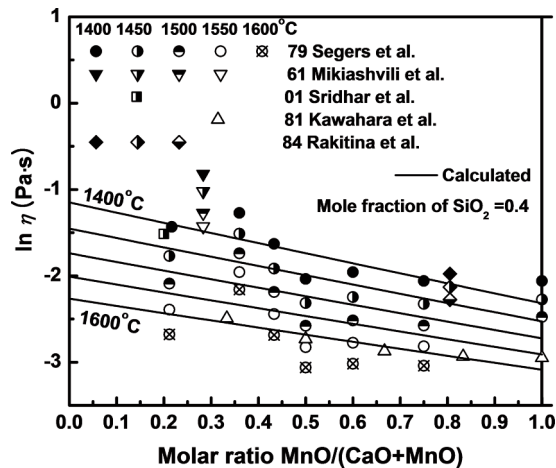


Figure 5. Viscosity of MnO-CaO-SiO₂ melts at 40 mol% SiO₂: experimental points [17, 24-27] and calculated lines.

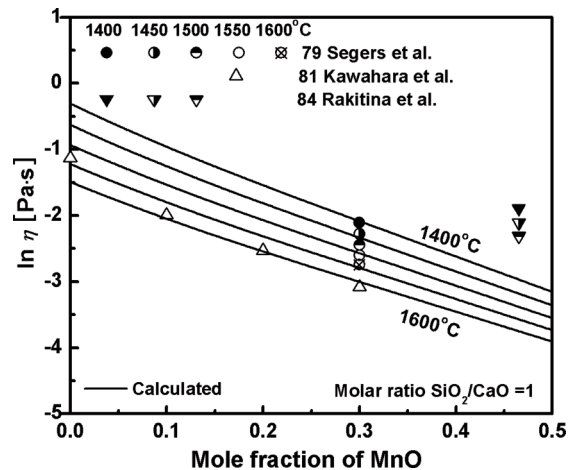


Figure 8. Viscosity of MnO-CaO-SiO₂ melts at a molar ratio SiO₂/CaO=1: experimental points [17, 25, 26] and calculated lines.

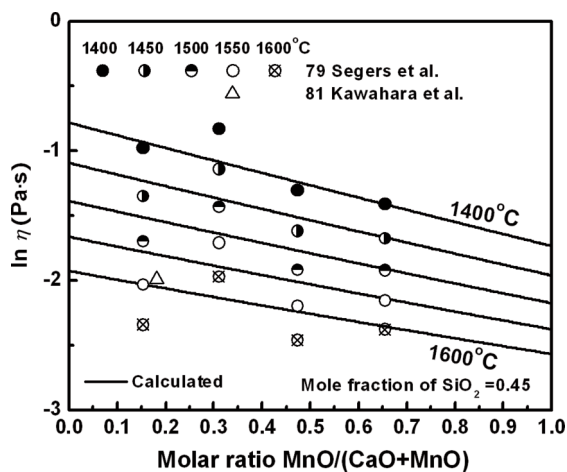


Figure 6. Viscosity of MnO-CaO-SiO₂ melts at 45 mol% SiO₂: experimental points [17, 25] and calculated lines.

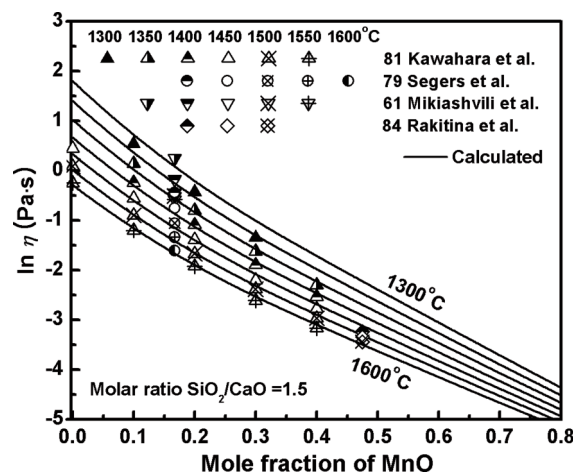


Figure 9. Viscosity of MnO-CaO-SiO₂ melts at a molar ratio SiO₂/CaO=1.5: experimental points [17, 24-26] and calculated lines.

3.3.2 MnO-Na₂O-SiO₂ and MnO-PbO-SiO₂

Experimental viscosity measurements in these systems are scarce and not very reliable. Ivanov et al. [28] and Artem'ev and Appen [29] measured the viscosity of MnO-Na₂O-SiO₂ melts using the rotating crucible method with Pt crucibles under Ar atmosphere. To the best of our knowledge, there is only one study of the viscosity of MnO-PbO-SiO₂ melts, which was done by the falling sphere method with Pt crucibles under Ar atmosphere [30]. These measurements are compared to the viscosities predicted by the model in Figs. 10 to 12. The agreement is believed to be within experimental error limits.

As can be seen from Fig. 10, Ivanov et al. [28] reported that the viscosity stays almost constant with increasing SiO₂ content, which is rather unlikely, whereas the model predicts increasing viscosity, as is to be expected.

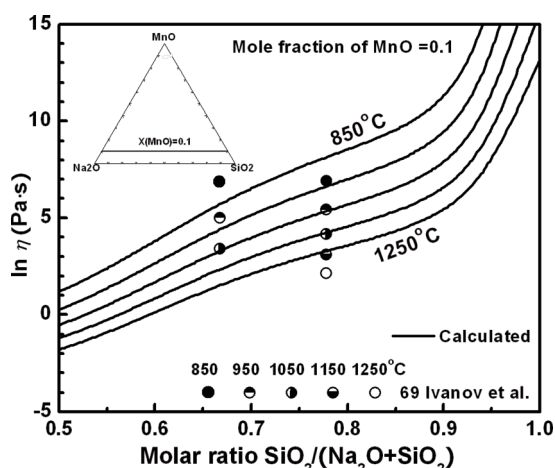


Figure 10. Viscosity of MnO-Na₂O-SiO₂ melts at 10 mol% MnO: experimental points [28] and calculated lines.

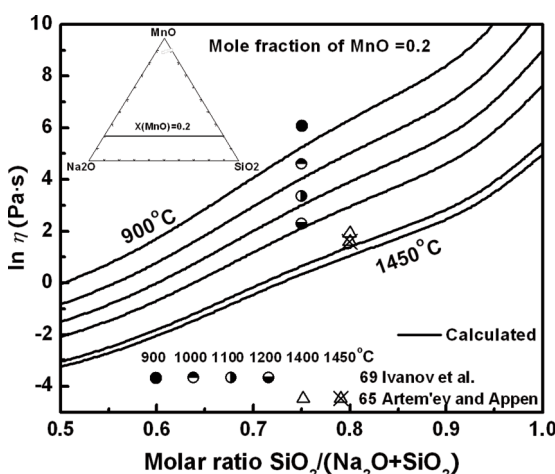


Figure 11. Viscosity of MnO-Na₂O-SiO₂ melts at 20 mol% MnO: experimental points [28, 29] and calculated lines.

It should be noted that the data of Nitta et al. [30] shown in Fig. 12 are systematically lower than the calculated lines for the composition corresponding to the binary PbO-SiO₂ system. Since the calculated lines describe very well numerous viscosity measurements in this binary system [8], the discrepancy is indicative of the experimental scatter which is at least 1.0 in the natural logarithmic scale.

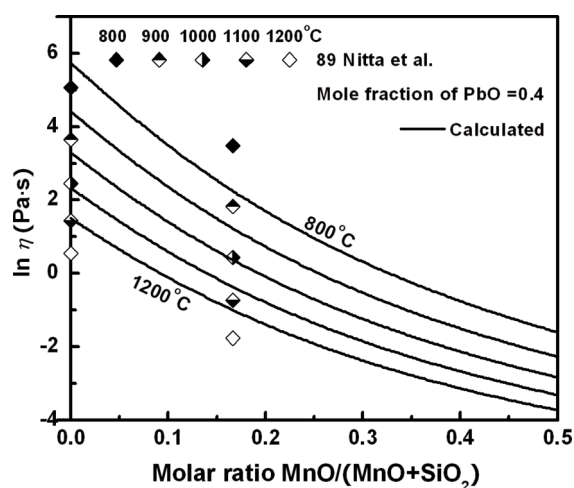


Figure 12. Viscosity of MnO-PbO-SiO₂ melts at 40 mol% PbO: experimental points [30] and calculated lines.

3.4 MnO-Al₂O₃-SiO₂

Mikiashvili et al. [19], Kawahara et al. [25], Urbain et al. [16] and Kou et al. [31] measured the viscosities of MnO-Al₂O₃-SiO₂ melts by the rotating crucible method with Mo [19], Pt [25] and Pt-Rh [16, 31] crucibles under Ar atmosphere. Towers and Gworek [22] used the logarithmic decrement method with Mo crucibles under (H₂+N₂) gas atmosphere. The studied compositions are shown in Figure 13. The experimental data are generally in good agreement, except for the viscosities obtained by Mikiashvili et al. [19] which tend to be higher than the results of other authors, especially at higher temperatures.

This system exhibits the Charge Compensation Effect which the viscosity model takes into account by assuming that tetrahedrally-coordinated Al, which enters the silica network and is charge-compensated by Mn, is formed by the reaction:

$$2\text{Al} + \text{Mn} \rightleftharpoons \text{MnAl}_2 \quad (13)$$

It is further assumed that the MnAl₂ “species” have the same effect on the viscosity as two Si atoms. The Gibbs energy of reaction (13) was optimized based on the experimental data for

MnO–Al₂O₃–SiO₂ melts mentioned above and is given in Table 1. The experimental and calculated viscosities are compared in Figs. 14 to 22 along the sections shown in Fig. 13.

A maximum in the viscosity originating from the Charge Compensation Effect is clearly visible in Fig. 17. Such maxima are observed in all studied MO_x–Al₂O₃–SiO₂ systems where M is an alkali or an alkaline-earth metal [2]. As can be seen from Figures 14 to 22, the model reproduces very well both the temperature and the composition dependence of the viscosity even though ΔG_{MnAl_2} is temperature independent.

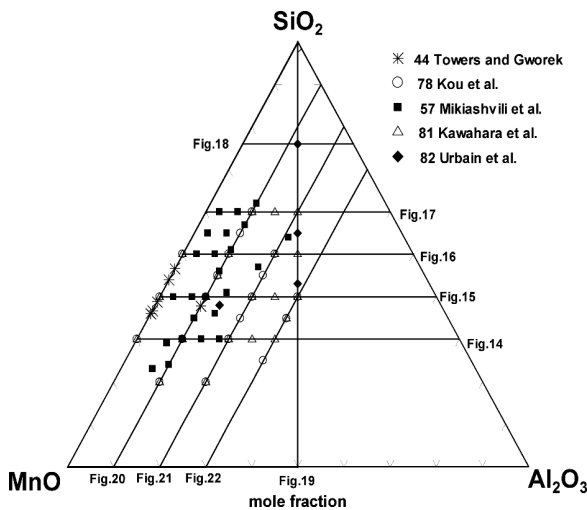


Figure 13. Compositions in the MnO–Al₂O₃–SiO₂ system at which experimental viscosity measurements are available [16, 19, 22, 25, 31]. The lines indicate nine sections of this system selected to show the viscosity as a function of composition in Figs 14 to 22.

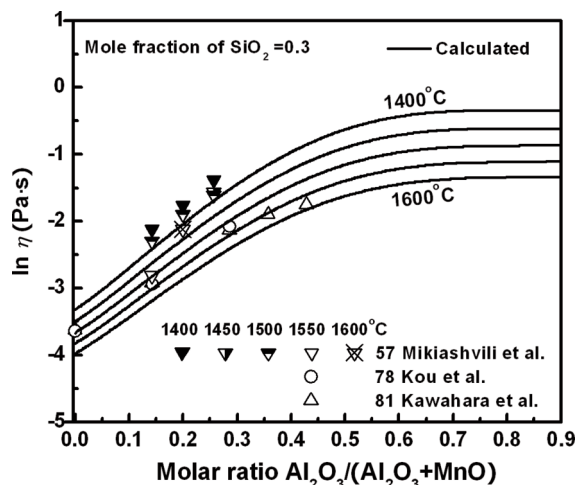


Figure 14. Viscosity of MnO–Al₂O₃–SiO₂ melts at 30 mol% SiO₂; experimental points [19, 25, 31] and calculated lines.

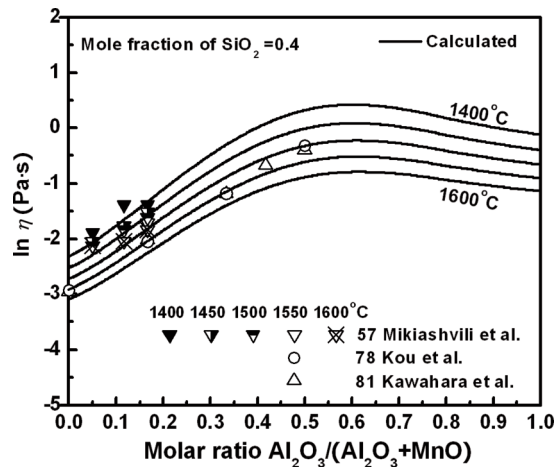


Figure 15. Viscosity of MnO–Al₂O₃–SiO₂ melts at 40 mol% SiO₂; experimental points [19, 25, 31] and calculated lines.

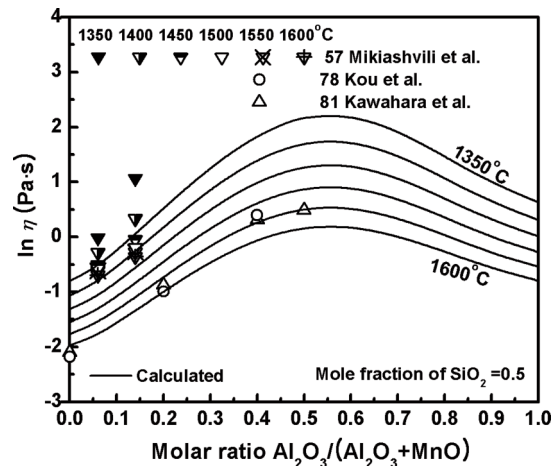


Figure 16. Viscosity of MnO–Al₂O₃–SiO₂ melts at 50 mol% SiO₂; experimental points [19, 25, 31] and calculated lines.

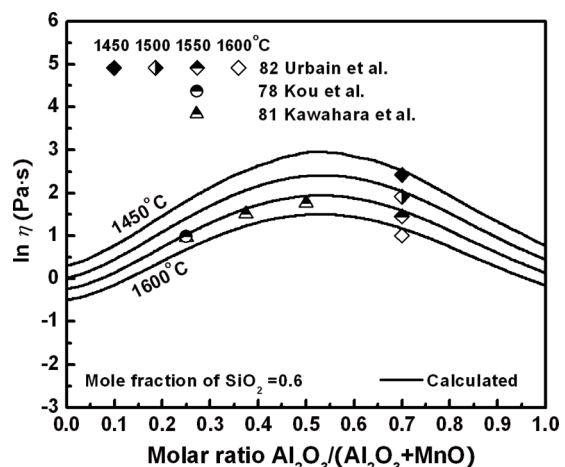


Figure 17. Viscosity of MnO–Al₂O₃–SiO₂ melts at 60 mol% SiO₂; experimental points [16, 25, 31] and calculated lines.

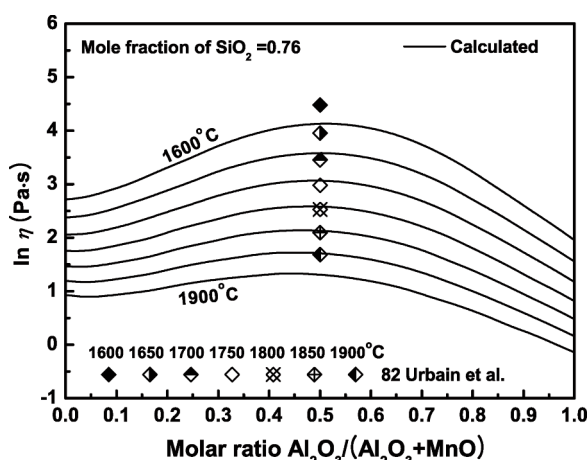


Figure 18. Viscosity of MnO- Al_2O_3 - SiO_2 melts at 76 mol% SiO_2 ; experimental points [16] and calculated lines.

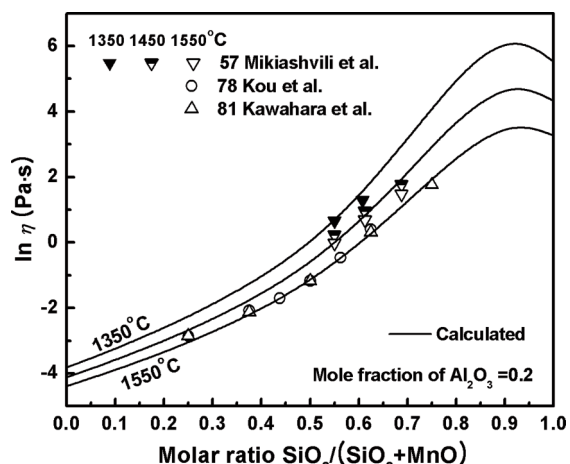


Figure 21. Viscosity of MnO- Al_2O_3 - SiO_2 melts at 20 mol% Al_2O_3 ; experimental points [19, 25, 31] and calculated lines.

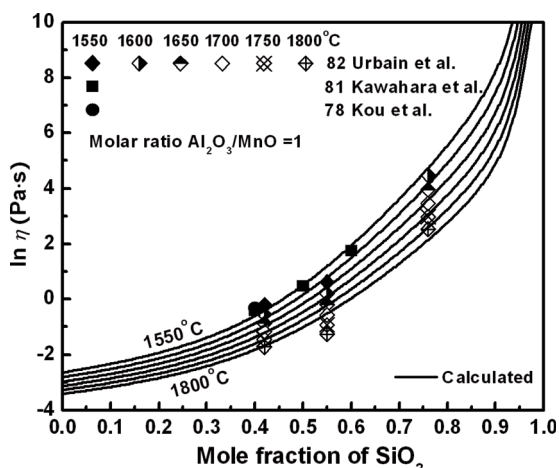


Figure 19. Viscosity of MnO- Al_2O_3 - SiO_2 melts at a molar ratio $\text{Al}_2\text{O}_3/\text{MnO} = 1$; experimental points [16, 25, 31] and calculated lines.

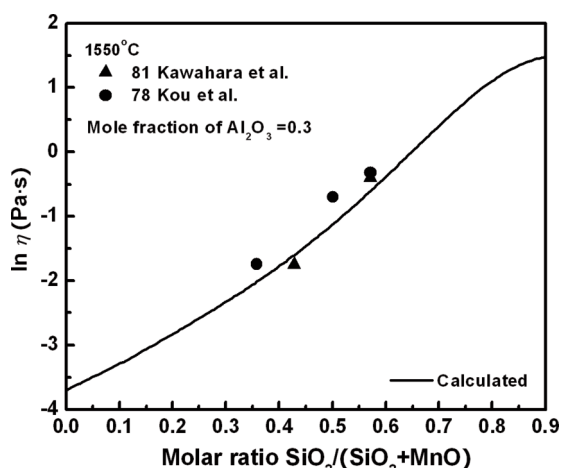


Figure 22. Viscosity of MnO- Al_2O_3 - SiO_2 melts at 30 mol% Al_2O_3 ; experimental points [25, 31] and calculated lines.

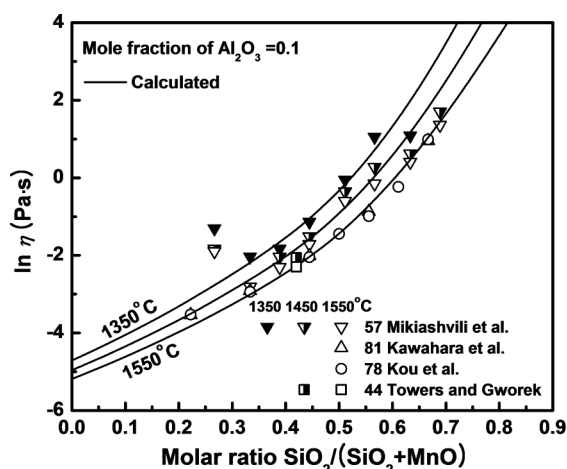


Figure 20. Viscosity of MnO- Al_2O_3 - SiO_2 melts at 10 mol% Al_2O_3 ; experimental points [19, 22, 25, 31] and calculated lines.

3.5 Multicomponent systems

The model contains unary parameters describing the viscosity of pure liquid oxides, binary parameters fitted to experimental viscosities of MO_x - SiO_2 melts and ternary parameters reproducing the viscosity of MO_x - Al_2O_3 - SiO_2 melts. The viscosity of multicomponent melts is predicted by the model without any additional adjustable model parameters.

To further test the predictive ability of the model, experimental viscosity data were collected for quaternary and multicomponent melts formed by MnO with SiO_2 , Al_2O_3 , CaO, MgO, PbO, Na_2O and K_2O . These data were not used for the calibration of our model.

3.5.1 MnO-CaO-MgO- SiO_2 system

Ji et al. [32] measured the viscosities of MnO-

CaO-MgO-SiO₂ melts using the rotating crucible method with iron crucibles and spindles under Ar atmosphere. As can be seen from Table 2, these data are in good agreement with the viscosities predicted by the model.

3.5.2 MnO-CaO-Al₂O₃-SiO₂ system

The viscosities of MnO-CaO-Al₂O₃-SiO₂ melts were measured by the rotating crucible method with iron crucibles under N₂ atmosphere [33], by the counter-balanced sphere method [34] and the falling sphere method [35] with Pt crucibles under Ar atmosphere, and by using a vibration viscometer with Mo crucibles under Ar atmosphere [36]. These data are compared with the viscosities predicted by the model in Figs. 23 to 26.

It should be noted that the model fits well the numerous viscosity data in the CaO-Al₂O₃-SiO₂ system [2]. Hence, the experimental scatter can be evaluated by extrapolation of the quaternary viscosity data to zero amount of MnO. (The left vertical axis in Figs. 23 to 26 corresponds to the CaO-Al₂O₃-SiO₂ system.) As can be seen from the figures, the results of Tanabe et al. [33] extrapolate to higher viscosities, while Kato and Minowa [34] reported lower viscosities for CaO-Al₂O₃-SiO₂ melts. The data of Takayanagi et al. [35] are in good agreement with the model for CaO-Al₂O₃-SiO₂ melts, but the viscosities of Chubinidze and Kekelidze [36] are in good agreement with the model only at higher temperatures and extrapolate to higher values at lower temperatures. As can be seen from Fig. 26, the spacing between the experimental points from the latter study indicates an irregular temperature dependence of the viscosity. This is most likely caused by precipitation of solid phases, since our phase equilibrium calculations show that the lowest temperatures reported by Chubinidze and Kekelidze [36] are below the liquidus. If the viscosity was measured on heating, solid phases may have remained in the melts even above the liquidus, resulting in overestimated viscosities.

Figures 23 to 26 demonstrate that the model correctly predicts the decrease of the viscosity as

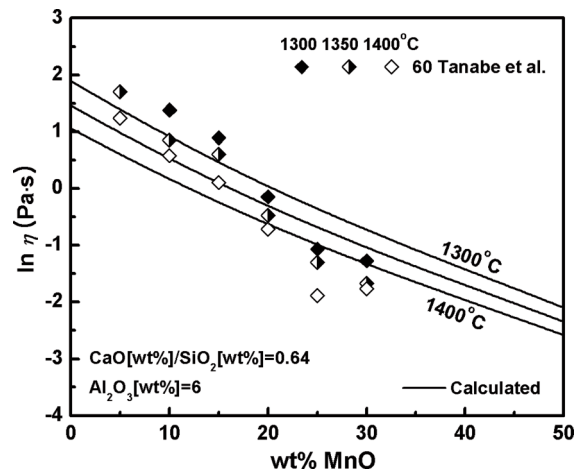


Figure 23. Viscosity of MnO-CaO-Al₂O₃-SiO₂ melts at 6 wt% Al₂O₃ and a weight ratio CaO/SiO₂=0.64: experimental points [33] and calculated lines.

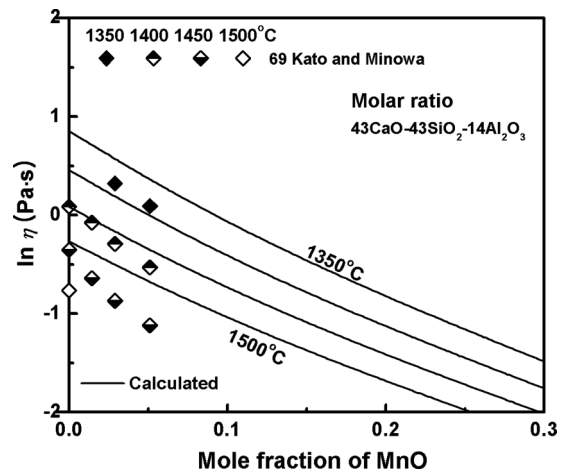


Figure 24. Viscosity of MnO-CaO-Al₂O₃-SiO₂ melts at a molar ratio of 43CaO-43SiO₂-14Al₂O₃: experimental points [34] and calculated lines.

Table 2. Viscosity of MnO-CaO-MgO-SiO₂ melts measured by Ji et al. [32] and predicted by the model.

SiO ₂ mol %	CaO mol %	MgO mol %	MnO mol %	Total mol %	Temperature °C	Viscosity, ln(Pa·s)		
						Ji et al. [32]	Present model	Difference
56.88	22.16	12.85	8.11	100	1335	-0.07	-0.1	0.03
43.54	7.18	24.97	24.32	100	1435	0.29	0.21	0.08
56.88	22.16	12.85	8.11	100	1450	1.22	0.89	0.33
43.54	7.18	24.97	24.32	100	1450	1.37	1	0.37
40.5	21.7	30.19	7.62	100	1450	-1.84	-1.68	-0.16
36.97	19.81	27.56	15.66	100	1480	-1.31	-1.8	0.49
40.5	21.7	30.19	7.62	100	1480	-1.58	-1.61	0.03
56.88	22.16	12.85	8.11	100	1500	-1.37	-1.51	0.14
43.54	7.18	24.97	24.32	100	1500	-1.02	-1.4	0.38

MnO is added to the system. This effect is minimal when MnO is substituted for CaO (see Fig. 26).

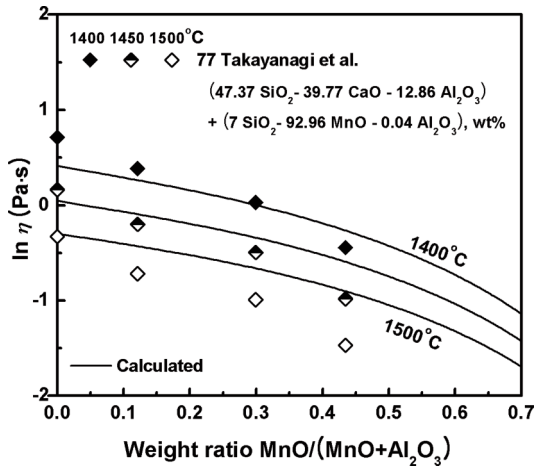


Figure 25. Viscosity of MnO-CaO-Al₂O₃-SiO₂ melts for a section between (47.37 wt% SiO₂, 39.77 wt% CaO, 12.86 wt% Al₂O₃) and (7 wt% SiO₂, 92.96 wt% MnO, 0.04 wt% Al₂O₃): experimental points [35] and calculated lines.

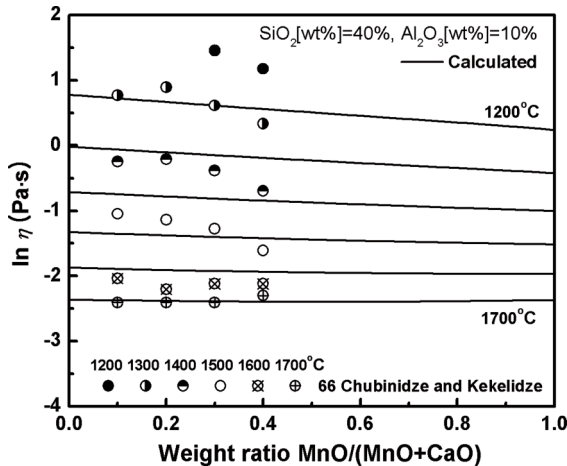


Figure 26. Viscosity of MnO-CaO-Al₂O₃-SiO₂ melts at 10 wt% Al₂O₃ and 40 wt% SiO₂: experimental points [36] and calculated lines.

3.5.3 MnO-CaO-MgO-Al₂O₃-SiO₂ system

Slags used for production of ferromanganese alloys belong to this five-component system. Therefore, several experimental viscosity studies were reported for these slags. Most researchers used the rotating crucible method with Mo [26, 37], Pt [38, 39] and graphite [40] crucibles under Ar [26, 37, 40], N₂ [38] or (H₂+N₂) [39] gas atmosphere.

The most extensive studies over wide composition ranges were reported by Persson [37] and Woollacott et al. [39]. These data are compared to the viscosities predicted by the model in Figs. 27 to 29 and in Table 3. The agreement is excellent; both the composition and

temperature dependence of the viscosity are adequately predicted by the model.

Rakitina et al. [26] measured the viscosities of three samples over the temperature range from 1300 to 1500 °C. The compositions of these samples are similar to the first composition in Table 3 studied by Persson [37]. At 1500 °C, the results of Rakitina et al. [26] are in good agreement with both the Persson's value and with the viscosities predicted by the model. However at 1400 and 1300 °C, the viscosities reported by Rakitina et al. [26] are substantially higher than predicted by the model. This is most likely due to precipitation of the monoxide solid solution in the experiments. Phase equilibrium calculations using the FactSage thermochemical software and oxide database [11] indicate that the liquidus temperatures for these compositions are much higher than 1400 °C.

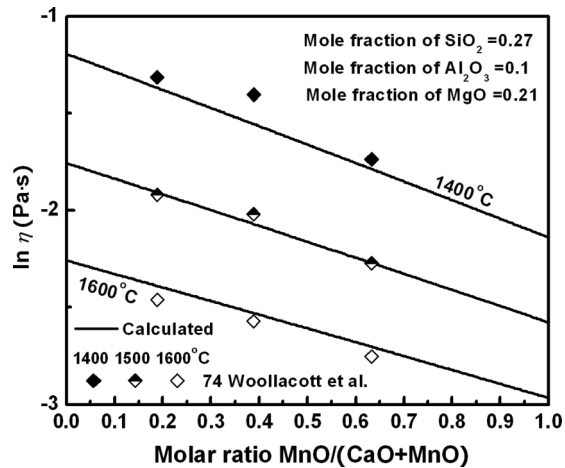


Figure 27. Viscosity of MnO-CaO-MgO-Al₂O₃-SiO₂ melts at 27 mol% SiO₂, 10 mol% Al₂O₃ and 21 mol% MgO: experimental points [39] and calculated lines.

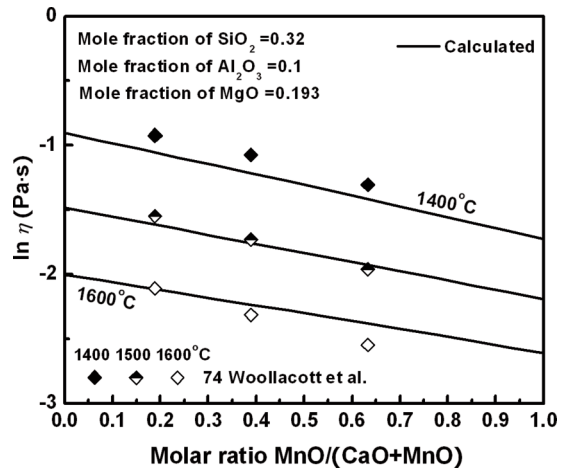


Figure 28. Viscosity of MnO-CaO-MgO-Al₂O₃-SiO₂ melts at 32 mol% SiO₂, 10 mol% Al₂O₃ and 19.3 mol% MgO: experimental points [39] and calculated lines.

Table 3. Viscosity of MnO-CaO-MgO-Al₂O₃-SiO₂ melts measured by Persson [37] and predicted by the model.

SiO ₂	CaO	MgO	Al ₂ O ₃	MnO	Total	Temp.	Viscosity, ln(Pa•s)		
mol	mol	mol	mol	mol	mol	°C	Persson	Present model	Difference
%	%	%	%	%	%		[37]		
22.5	17.5	7.1	6.1	46.9	100	1489	-3.02	-3.19	0.17
22.5	17.5	7.1	6.1	46.9	100	1603	-3.38	-3.61	0.23
22.5	17.5	7.1	6.1	46.9	100	1703	-3.55	-3.94	0.39
26.9	20.8	8.3	7.1	36.8	100	1302	-1.85	-1.76	-0.09
26.9	20.8	8.3	7.1	36.8	100	1496	-2.74	-2.7	-0.04
26.9	20.8	8.3	7.1	36.8	100	1608	-3.1	-3.15	0.05
26.9	20.8	8.3	7.1	36.8	100	1706	-3.28	-3.5	0.22
31.1	24	9.6	8.1	27.2	100	1302	-0.99	-1.16	0.17
31.1	24	9.6	8.1	27.2	100	1399	-1.64	-1.7	0.06
31.1	24	9.6	8.1	27.2	100	1504	-2.2	-2.23	0.03
31.1	24	9.6	8.1	27.2	100	1603	-2.66	-2.67	0.01
31.1	24	9.6	8.1	27.2	100	1698	-2.99	-3.04	0.05
17.2	13.6	0.6	17.3	51.3	100	1397	-2.34	-2.56	0.22
17.2	13.6	0.6	17.3	51.3	100	1500	-2.75	-2.98	0.23
17.2	13.6	0.6	17.3	51.3	100	1605	-3.12	-3.36	0.24
20.8	16.4	0.6	21.1	41.1	100	1399	-2.02	-1.92	-0.1
20.8	16.4	0.6	21.1	41.1	100	1498	-2.44	-2.37	-0.07
20.8	16.4	0.6	21.1	41.1	100	1604	-2.87	-2.8	-0.07
24.2	19.3	1.1	23.4	32	100	1439	-1.35	-1.57	0.22
24.2	19.3	1.1	23.4	32	100	1500	-1.77	-1.87	0.1
24.2	19.3	1.1	23.4	32	100	1602	-2.28	-2.32	0.04
26.2	4.7	2.7	16.7	49.8	100	1407	-2.09	-2.04	-0.05
26.2	4.7	2.7	16.7	49.8	100	1503	-2.46	-2.46	0
26.2	4.7	2.7	16.7	49.8	100	1605	-2.87	-2.86	-0.01
32.1	5.7	3.2	19	40	100	1404	-1.26	-1.2	-0.06
32.1	5.7	3.2	19	40	100	1507	-1.78	-1.72	-0.06
32.1	5.7	3.2	19	40	100	1601	-2.21	-2.14	-0.07
38.3	6.1	3.8	20	31.8	100	1395	-0.32	-0.26	-0.06
38.3	6.1	3.8	20	31.8	100	1501	-1.13	-0.89	-0.24
38.3	6.1	3.8	20	31.8	100	1603	-1.81	-1.43	-0.38
20.3	28.5	9.3	5.9	35.9	100	1507	-3.46	-3.13	-0.33
20.3	28.5	9.3	5.9	35.9	100	1603	-3.65	-3.5	-0.15
22.8	31.8	10.3	7	28.2	100	1506	-2.86	-2.78	-0.08
22.8	31.8	10.3	7	28.2	100	1602	-3.21	-3.18	-0.03

Figures 30 and 31 compare the experimental data of Semik [40] and Vulchev and Todorov [38] with the viscosities predicted by the model. As can be seen from Fig. 30, the results of Semik [40] are in good agreement

with the model above the liquidus, but become increasingly higher as temperature drops below the liquidus, indicating possible precipitation of the spinel solid solution in the experiments. Similarly, the

composition dependence of the viscosity predicted by the model is in reasonable agreement with the measurements of Vulchev and Todorov [38] above the liquidus, even though the experimental data are systematically higher than the calculated lines by about 0.9 in the natural logarithmic scale. However, the experimental results below the liquidus are most likely affected by precipitation of solid phases.

Kurnushko [41] measured the viscosities of five MnO-CaO-MgO-Al₂O₃-SiO₂ melts using a vibrational viscometer with Mo crucibles under N₂ atmosphere. His data are systematically higher (from 0.8 to 2.3 in the natural logarithmic scale) than the calculated viscosities at all temperatures and compositions. Again, one

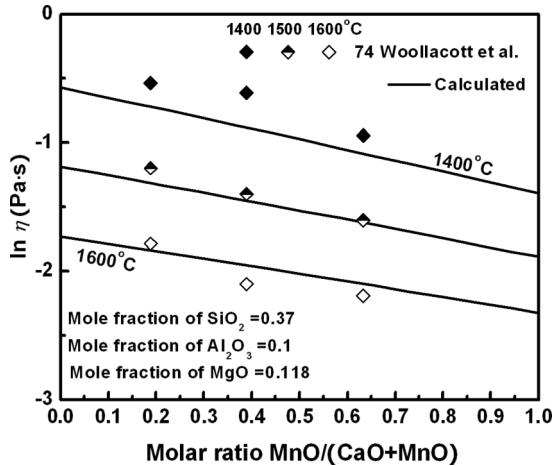


Figure 29. Viscosity of MnO-CaO-MgO-Al₂O₃-SiO₂ melts at 37 mol% SiO₂, 10 mol% Al₂O₃ and 11.8 mol% MgO: experimental points [39] and calculated lines.

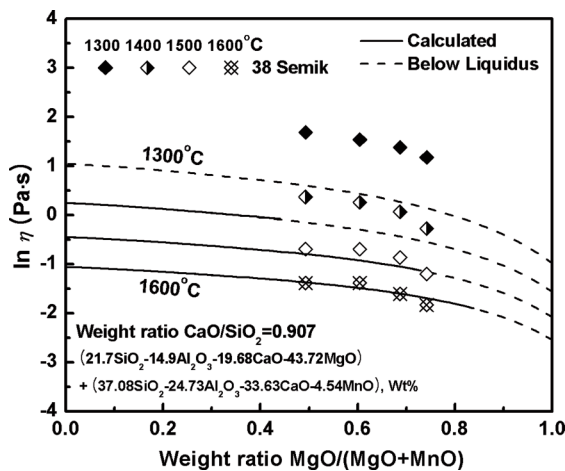


Figure 30. Viscosity of MnO-CaO-MgO-Al₂O₃-SiO₂ melts for a section between (21.7 mol% SiO₂, 14.9 mol% Al₂O₃, 19.68 mol% CaO, 43.72 mol% MgO) and (37.08 mol% SiO₂, 24.73 mol% Al₂O₃, 33.63 mol% CaO, 4.54 mol% MnO) with a weight ratio CaO/SiO₂=0.907: experimental points [40] and calculated lines.

possible explanation of this disagreement is precipitation of the alpha-Ca₂SiO₄ solid solution which can dissolve some Mg₂SiO₄ and Mn₂SiO₄.

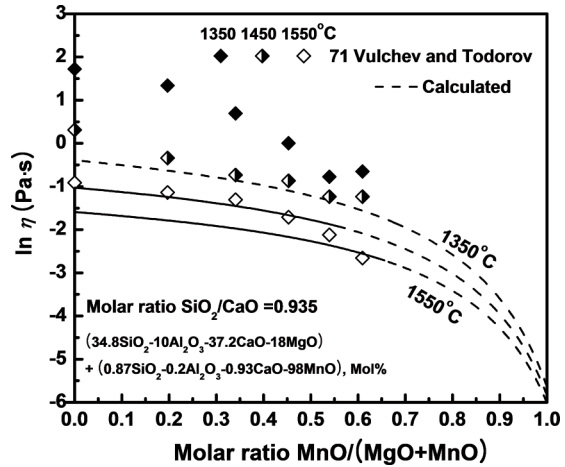


Figure 31. Viscosity of MnO-CaO-MgO-Al₂O₃-SiO₂ melts for a section between (34.8 mol% SiO₂, 10 mol% Al₂O₃, 37.2 mol% CaO, 18 mol% MgO) and (0.87 mol% SiO₂, 0.2 mol% Al₂O₃, 0.93 mol% CaO, 98 mol% MnO) with a molar ratio SiO₂/CaO=0.935: experimental points [38] and calculated lines.

3.5.4 MnO-K₂O-CaO-Al₂O₃-SiO₂ system

The viscosities of MnO-K₂O-CaO-Al₂O₃-SiO₂ melts were measured only by Rudneva et al. [42] who used the rotating crucible method with graphite crucibles under N₂ atmosphere. Calculated viscosities are compared with the experimental data in Fig. 32.

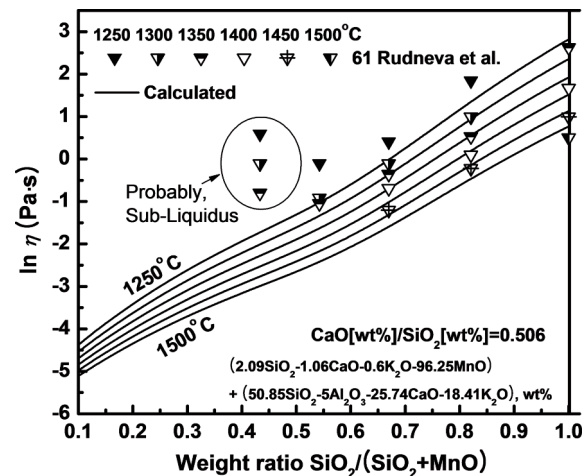


Figure 32. Viscosity of MnO-K₂O-CaO-Al₂O₃-SiO₂ melts for a section between (2.09 wt% SiO₂, 1.06 wt% CaO, 0.60 wt% K₂O, 96.25 wt% MnO) and (50.85 wt% SiO₂, 5.00 wt% Al₂O₃, 25.74 wt% CaO, 18.41 wt% K₂O) with a weight ratio CaO/SiO₂=0.506: experimental points [42] and calculated lines.

As almost pure MnO is added to the master SiO₂-Al₂O₃-CaO-K₂O melt, the viscosity decreases. This is mostly due to the decrease in the silica content. The slope of this decrease is well predicted by the model. However, the measurements for the most MnO-rich composition contradict this trend and suggest an abrupt increase in the viscosity. Since it is very difficult to rationalize such an increase, it was most likely caused by precipitation of solid phases in the experiment.

3.5.5 MnO-Na₂O-K₂O-CaO-MgO-Al₂O₃-SiO₂ system

Table 4 compares the viscosities of MnO-Na₂O-K₂O-CaO-MgO-Al₂O₃-SiO₂ melts predicted by the model with the measurements of Tkach et al. [43] who used a vibrational viscometer under Ar atmosphere. As can be seen from Table 4, the experimental data are systematically lower than the calculated viscosities. It should be noted that a systematic error of about 1.0 in the natural logarithmic scale is fairly common. The temperature dependence of the viscosity for each of the three studied samples is well described by the model.

4. Conclusions

To calculate the viscosity of MnO-containing silicate melts, only six model parameters related to MnO are required. Two parameters, A_{Mn} and E_{Mn} , describe the viscosity of pure liquid MnO; two binary parameters, E_{Mn-Si} and E_{Mn-Si}^R , describe the viscosity of MnO-SiO₂ melts; and, finally, two more parameters represent the Gibbs energy, ΔG_{MnAl} , of tetrahedrally-coordinated Al "species" which enter the silica network and are charge-compensated by Mn. The latter two parameters are obtained from the experimental viscosities of MnO-Al₂O₃-SiO₂ melts. The viscosities of multicomponent melts containing MnO are then predicted by the model without any additional adjustable model parameters.

To test the model, available experimental viscosity data were collected for melts formed by MnO with SiO₂, Al₂O₃, CaO, MgO, PbO, Na₂O and K₂O. The deviation of the available experimental data from the viscosities predicted by the model does not exceed the scatter of experimental points among different authors in binary and ternary sub-systems of the MnO-SiO₂-Al₂O₃-CaO-MgO-PbO-Na₂O-K₂O system that were used to calibrate the model.

Table 4. Viscosity of MnO-CaO-MgO-Na₂O-K₂O-Al₂O₃-SiO₂ melts measured by Tkach et al. [43] and predicted by the model.

SiO ₂	CaO	MgO	Al ₂ O ₃	MnO	Na ₂ O	K ₂ O	Total	Temp.	Viscosity, ln(Pa·s)		
wt %	wt %	wt %	wt %	wt %	wt %	wt %	wt %	°C	Tkach et al. [43]	Present model	Difference
51.3	12.8	4.4	9.1	16.8	2.9	2.8	100.1	1400	0.21	1.12	-0.91
51.3	12.8	4.4	9.1	16.8	2.9	2.8	100.1	1450	-0.35	0.76	-1.11
51.3	12.8	4.4	9.1	16.8	2.9	2.8	100.1	1500	-0.74	0.41	-1.15
51.3	12.8	4.4	9.1	16.8	2.9	2.8	100.1	1550	-1.11	0.09	-1.2
51.3	12.8	4.4	9.1	16.8	2.9	2.8	100.1	1600	-1.27	-0.22	-1.05
50.4	12.8	4.3	10.4	17	2.2	2.3	99.4	1400	0.11	1.07	-0.96
50.4	12.8	4.3	10.4	17	2.2	2.3	99.4	1450	-0.28	0.71	-0.99
50.4	12.8	4.3	10.4	17	2.2	2.3	99.4	1500	-0.69	0.36	-1.05
50.4	12.8	4.3	10.4	17	2.2	2.3	99.4	1550	-1.04	0.04	-1.08
50.4	12.8	4.3	10.4	17	2.2	2.3	99.4	1600	-1.26	-0.27	-0.99
48.5	12.8	4	11.4	18.4	1.3	3.1	99.5	1400	0.22	0.88	-0.66
48.5	12.8	4	11.4	18.4	1.3	3.1	99.5	1450	-0.17	0.52	-0.69
48.5	12.8	4	11.4	18.4	1.3	3.1	99.5	1500	-0.54	0.18	-0.72
48.5	12.8	4	11.4	18.4	1.3	3.1	99.5	1550	-0.82	-0.14	-0.68
48.5	12.8	4	11.4	18.4	1.3	3.1	99.5	1600	-0.98	-0.44	-0.54

In particular, the model predicts the viscosity of MnO-CaO-MgO-Al₂O₃-SiO₂ slags used for production of ferromanganese alloys with an accuracy similar to the accuracy of the experimental studies of these melts.

Acknowledgements

Financial assistance from the Natural Sciences and Engineering Research Council of Canada (NSERC) through a Discovery grant is gratefully acknowledged.

References

- [1] A.N. Grundy, H.-C. Liu, I.-H. Jung, S.A. Decterov, A.D. Pelton, *Int. J. Mat. Res.*, 99 (11) (2008) 1185-1194.
- [2] A.N. Grundy, I.-H. Jung, A.D. Pelton, S.A. Decterov, *Int. J. Mat. Res.*, 99 (11) (2008) 1195-1209.
- [3] W.-Y. Kim, A.D. Pelton, S.A. Decterov, *Int. J. Mat. Res.*, 103 (3) (2012) 313-328.
- [4] E. Brosh, A.D. Pelton, S.A. Decterov, *Int. J. Mat. Res.*, 103 (4) (2012) 494-501.
- [5] E. Brosh, A.D. Pelton, S.A. Decterov, *Int. J. Mat. Res.*, 103 (5) (2012) 537-550.
- [6] A.D. Pelton, S.A. Decterov, G. Eriksson, C. Robelin, Y. Dessureault, *Metall. Mater. Trans. B*, 31B (4) (2000) 651-659.
- [7] A.D. Pelton, P. Chartrand, *Metall. Mater. Trans. A*, 32A (6) (2001) 1355-1360.
- [8] W.-Y. Kim, A.D. Pelton, S.A. Decterov, *Metallurgical and Materials Transactions B: Process Metallurgy and Materials Processing Science*, 43 (2) (2012) 325-336.
- [9] W.-Y. Kim, X. Yang, L. Yan, A.D. Pelton, S.A. Decterov, *Calphad*, 35 (4) (2011) 542-550.
- [10] B. Mysen, *Eur. J. Mineral.*, 15 (5) (2003) 781-802.
- [11] C.W. Bale, E. Belisle, P. Chartrand, S.A. Decterov, G. Eriksson, K. Hack, I.-H. Jung, Y.-B. Kang, J. Melancon, A.D. Pelton, C. Robelin, S. Petersen, *Calphad*, 33 (2) (2009) 295-311.
- [12] W.J. Malfait, W.E. Halter, Y. Morizet, B.H. Meier, R. Verel, *Geochim. Cosmochim. Acta*, 71 (24) (2007) 6002-6018.
- [13] D.W. Matson, S.K. Sharma, J.A. Philpotts, *J. Non-Cryst. Solids*, 58 (2-3) (1983) 323-352.
- [14] S. Vargas, F.J. Frandsen, K. Dam-Johansen, *Progress in Energy and Combustion Science*, 27 (3) (2001) 237-429.
- [15] K.C. Mills, L. Chapman, A.B. Fox, S. Sridhar, *Scand. J. Metall.*, 30 (6) (2001) 396-403.
- [16] G. Urbain, Y. Bottinga, P. Richet, *Geochim. Cosmochim. Acta*, 46 (6) (1982) 1061-1072.
- [17] L. Segers, A. Fontana, R. Winand, *Electrochim. Acta*, 24 (2) (1979) 213-218.
- [18] S. Yagi, K. Mizoguchi, Y. Suginothara, *Kyushu Kogyo Daigaku Kenkyu Hokoku, Kogaku*, 40 (1980) 33-38.
- [19] S.M. Mikiashvili, L.M. Tsylev, A.M. Samarin, *Fiz-Khim. Osnovy Proizvodstva Stali, Akad. Nauk S.S.S.R., Inst. Met. im. A. A. Baikova, Trudy 3-ei Konf.* (1957), Volume Date 1955, (1957) 423-432.
- [20] V.I. Sokolov, S.I. Popel, O.A. Esin, *Izvestiya Vysshikh Uchebnykh Zavedenii, Chernaya Metallurgiya*, 13 (4) (1970) 40-45.
- [21] J.R. Rait, Q.C. M'Millan, R. Hay, *J. R. Technol. College*, 4 (1939) 449-466.
- [22] H. Towers, J.M. Gworek, *J. West Scot. Iron Steel Inst.*, 51 (1944) 123-133.
- [23] D.T. Livey, H. Towers, H.B. Bell, R. Hay, *Trans. Br. Ceram. Soc.*, 53 (1954) 741-747.
- [24] S.M. Mikiashvili, A.Y. Arsenishvili, A.G. Bukhrashvili, *Soobshcheniya Akademii Nauk Gruzinskoi SSR*, 27 (1961) 313-320.
- [25] M. Kawahara, K. Mizoguchi, Y. Suginothara, *Kyushu Kogyo Daigaku Kenkyu Hokoku, Kogaku*, 43 (1981) 53-59.
- [26] N.I. Rakitina, N.A. Turkina, A.A. Morozov, V.Y. Dashevskii, I.A. Karyazin, V.I. Kashin, *Izv. Akadem. Nauk SSSR, Metall.*, 1 (1984) 28-32.
- [27] S. Sridhar, D. Sichen, S. Seetharaman, K.C. Mills, *Steel Res.*, 72 (1) (2001) 3-10.
- [28] O.G. Ivanov, N.I. Tret'yakova, O.V. Mazurin, *Steklo i Keramika*, 26 (7) (1969) 42-45.
- [29] V.I. Artem'ev, A.A. Appen, *Zh. Prikl. Khim. (S.-Peterburg, Russ. Fed.)*, 38 (2) (1965) 409-411.
- [30] A. Nitta, T. Miura, T. Komatsu, K. Matusita, *J. Am. Ceram. Soc.*, 72 (1) (1989) 163-165.
- [31] T. Kou, K. Mizoguchi, Y. Suginothara, *Nippon Kinzoku Gakkaishi*, 42 (8) (1978) 775-781.
- [32] F.-Z. Ji, D. Sichen, S. Seetharaman, *Int. J. Thermophys.*, 20 (1) (1999) 309-323.
- [33] I. Tanabe, K. Oku, T. Honda, *Denki Kagaku*, 28 (12) (1960) 681-686.
- [34] M. Kato, S. Minowa, *Trans. Iron Steel Inst. Jpn.*, 9 (1) (1969) 31-38.
- [35] T. Takayanagi, M. Kato, S. Minowa, *Imono*, 49 (1) (1977) 9-13.
- [36] T.A. Chubinidze, M.A. Kekelidze, *Soobshcheniya Akademii Nauk Gruzinskoi SSR*, 43 (3) (1966) 667-674.
- [37] M. Persson, *Investigation of Slag Properties and Reactions*, in, *Doctoral Thesis, Royal Institute of Technology, Stockholm, Sweden, 2007*, pp. 90 pp.
- [38] I. Vulchev, K. Todorov, *Godishnik na Visshiya Khimikotekhnologicheski Institut, Sofiya*, 16 (1) (1971) 107-119.
- [39] L.C. Woollacott, D.D. Howat, P.R. Joches, *Proceedings of INFACON '74: The first International Congress on Ferro-Alloys, Johannesburg, South Africa, (1974)* 227-232.
- [40] I.P. Semik, *Sovetskaya Metallurgiya*, 10 (2) (1938) 22-34.
- [41] O.V. Kurnushko, *Fiz.Khim. Osnovy Proizv. Stali, Akad. Nauk SSSR, Inst. Met., Tr. 6-oi [Shestoi] Konf., Moscow, 1961 (1964)* 158-168.
- [42] A.V. Rudneva, N.L. Zhilo, I.I. Gul'tyai, G.A. Sokolov, *Trudy Inst. Met. im. A. A. Baikova*, 8 (1961) 11-29.
- [43] G.D. Tkach, A.G. Kucher, M.I. Gasik, *Izvestiya Vysshikh Uchebnykh Zavedenii, Chernaya Metallurgiya*, 10 (1976) 68-70.